

Magnetic Merry Go Round - Resonant Reshaping of Colloidal Clusters on a Current Carrying Wire

Lydiane Becu¹, Marc Basler², Miodrag L. Kulić^{3,4}, and Igor M. Kulić^{2*}

¹*Université de Lorraine, LCP-A2MC, Institut de Chimie,*

Physique et Matériaux, 1 Bd. Arago, 57070 Metz, France

²*CNRS, Institute Charles Sadron, 23 rue du Loess BP 84047, 67034 Strasbourg, France*

³*Institute for Theoretical Physics, Goethe-University D-60438 Frankfurt am Main, Germany and*

⁴*Institute of Physics, Belgrade, Serbia*

(Dated: October 5, 2018)

We describe a simple physical method for trapping and transforming magnetic colloid clusters on a current carrying wire. We use the wire's field as a mould to form colloidal rings and helices on its surface. To transform the initially amorphous, kinetically trapped, bulky clusters we induce a low frequency magnetic modulation wave that spins around the wire axis, effectively eliminates defects from the clusters and stretches them into slender rings and helical structures. A qualitative theoretical model of the underlying resonant transformations is developed and the practical potential of the wire as a magnetic micro-assembler is discussed.

PACS numbers: 82.70.Dd, 81.16.Dn, 82.70.Rr

INTRODUCTION

Assembling controlled super-structures on the micro- and nanoscale is among the current challenges in colloidal science. Many original methods to guide the formation of well-defined colloidal structures have been invented, including assembly of colloidal rings at interfaces [1] and in ferrofluids [2], colloidal helices via chiral templating [3] and complex Janus particle interactions [4]. Effective interactions between magnetic beads via dynamic magic angle spinning [5], giving rise to novel many body, Van der Waals-like interactions [6] have been utilized in forming self-healing membranes and foams [7] that are finding first applications in templating cellular tissue growth [8].

In contrast to the equilibrium, thermally driven self-assembly, the process of a non-equilibrium field driven assembly induces interactions that are often stronger than the thermal energy scale [9]. If the energy landscape is sufficiently simple and smooth, large field driven, effective interactions can speed up and direct the kinetics and furthermore open pathways to new dissipative structures, and non-equilibrium steady states [10, 11]. However, in most cases where the energy landscape is rugged and has many meta-stable states, large barriers effectively prevent the system from finding a unique configuration in experimentally practical times. Lacking the simplifying principle of free energy minimization one is forced to resort to new ideas for guiding the colloidal assemblies to their desired final structure.

In this paper we expand the repertoire of ideas for tailoring colloidal clusters by a new dynamical mechanism. We force randomly formed clusters into desired shapes - in our case colloidal rings- by applying out-of-equilibrium forces via dynamic fields. Linear colloidal super-structures like rings and helices have an esthetic appeal. Yet, owing to their non-straight geometry, they

appear notoriously difficult to generate. Despite minimizing magnetic energy, magnetic rings are rarely observed spontaneously [12] and require spacial conditions, like confinement on solid surfaces [2] and liquid interfaces [1] to form. One interesting idea that we stumbled upon and present in this paper is to use a "field moulding" method on a current carrying wire : Linear colloidal super-structures are expected to follow imposed magnetic field lines. Thus, by controlling field lines we control the cluster geometry itself. A simple current carrying wire and the Biot-Savart circular field structure around them appear as a natural candidate to form rings. However along this avenue, once again, we quickly meet the roadblock posed by kinetic traps in the complex space of colloidal cluster configurations.

In this work we report on a method to overcome this kinetic problem by introducing what we call a "*magnetic merry-go-round field*" - a rotating field, dynamically modulating the Biot-Savart field - around the wire axis that effectively stretches the amorphous clusters into rings and helices. In the first part of the paper we present the basic geometry of the setup and the induced dynamic fields, as well as their effects on cluster reshaping. In a second part we theoretically rationalize for the experimentally observed cluster reshaping behavior by developing a simplified, analytically tractable dimer toy-model. We conclude with an outlook giving a glimpse of further possibilities of the wire trap and ideas that could be explored in the future.

MATERIALS AND METHODS

Superparamagnetic Beads. The experiments were performed with superparamagnetic beads consisting of a polystyrene polymer matrix doped with magnetite nano-

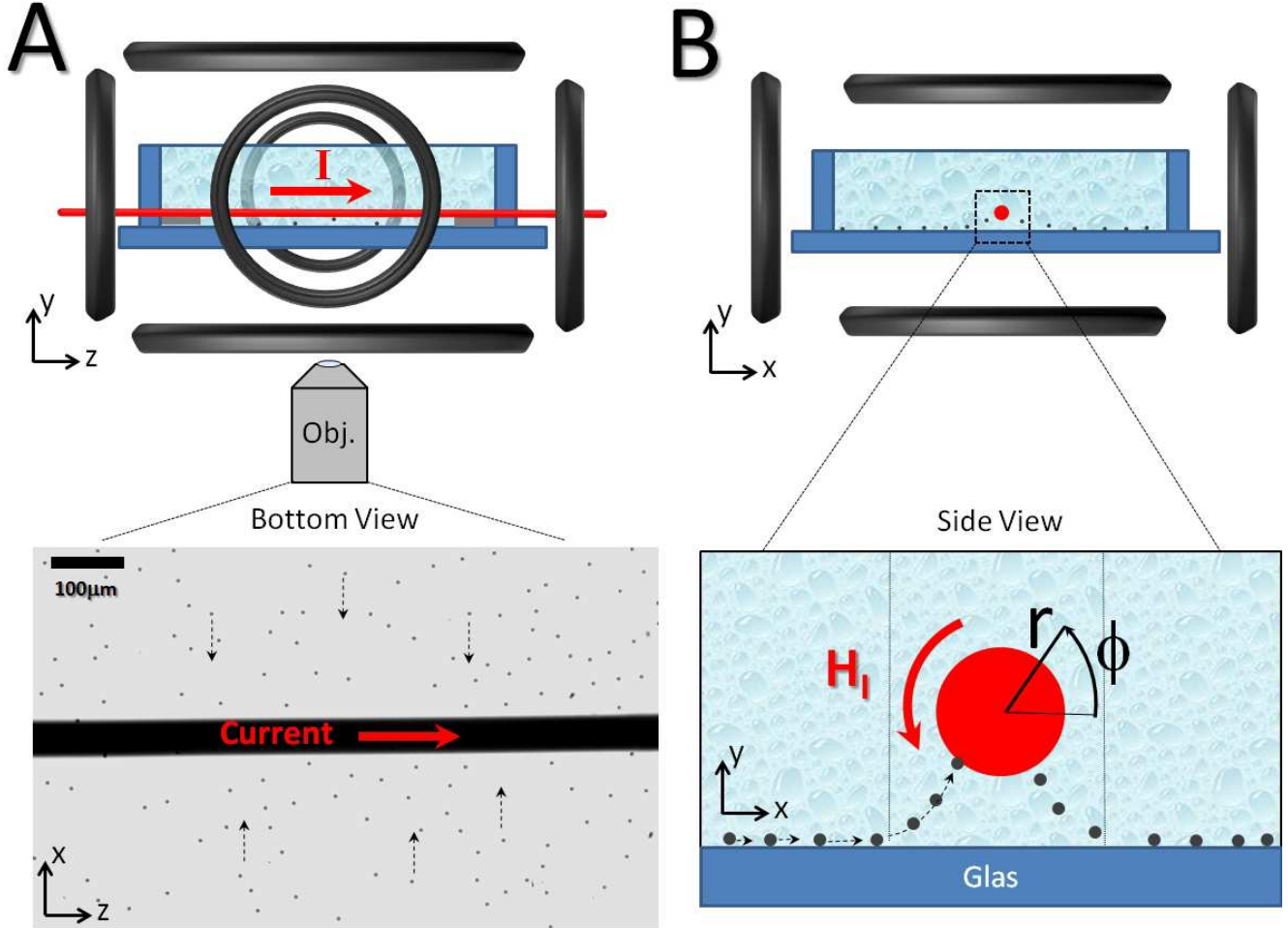


FIG. 1: The wire trap experimental setup : A $50\mu\text{m}$ current carrying copper wire suspended over a glass substrate traps superparamagnetic beads. Additional pairs Helmholtz coils induce uniform fields in the x , y and z direction that modulate the field of the wire.

crystals (Dynabeads M-450, Invitrogen). In order to prevent aggregation and surface adhesion, the superparamagnetic particles were suspended in a 5.9×10^{-3} M sodium dodecyl sulfate solution [17]. The beads have a diameter $d_b(\equiv 2r_b) = 4.4\mu\text{m}$, a mass density $\rho_b = 1.5 \times 10^3 \text{kg/m}^3$ and the magnetic bead susceptibility $\tilde{\chi}_b = 6.2 \times 10^{-11} \text{Am}^2/\text{T}$, [18]. The latter is related to the dimensionless bead susceptibility $\chi_b = \mu_0 \tilde{\chi}_b / V_b = 1.75$, with $\mu_0 = 4 \times 10^{-7} \text{Tm/A}$ the magnetic permeability of vacuum and $V_b = \frac{\pi}{6} d_b^3$ the beads volume. Susceptibilities are defined as a response function of the magnetization M or the magnetic moment $m = MV_b$ to the external magnetic field $m = \tilde{\chi}_b B_e = \chi_b V_b H_e$ and $M = \chi_b H_e$. In the following we omit the index in B_e and H_e .

Bead trapping on the wire - The colloidal suspension is placed inside a silicone chamber (Coverwell perfusion chamber, height 1 mm) that was glued to a microscope glass slide. Due to their large density the colloidal beads sediment on the microscope glass slide. An uninsulated

copper wire (diameter $d_w(\equiv 2r_w) = 50\mu\text{m}$ connected to a constant current generator passes through the experimental cell, as sketched in Fig. (1). Spacers of height $\approx 100\mu\text{m}$ ensured that the wire is suspended above the microscope slide surface, and its height h was measured before each experiment. In order to generate magnetic fields able to attract particles at the surface of the wire, significant currents must go through the wire, generating high current densities up to $200 - 300 \text{A/mm}^2$, giving rise to fields of several mT -at the wire surface). The thin wire could support currents up to 0.5A for several minutes and up to 0.8A for short times without deterioration.

The high currents through such thin wires can be achieved due to a more efficient heat dissipation on the surface of micrometric wires in aqueous solutions. The Joule-heating power per length of a wire of radius r_w scales as $P_J/l \sim \rho r_w^{-2} I^2$ with ρ the specific resistivity, while the dissipated power due to advection cooling

$P_C/l \sim r_w h \Delta T$ with h the heat transfer coefficient and ΔT the temperature difference between the wire and the solvent (in the bulk). To maintain a small limited temperature difference ΔT , the power balance $P_J = P_C$ implies a maximal current scaling as $I^2 \sim \rho_w^{-1} r^3 h \Delta T$.

Additional fields generated by a set of commercial and custom made Helmholtz coils along the x, y or the z direction were superimposed with the field of the wire. The coils were driven by a computer controlled signal generator linked to a custom amplifier that allows to choose the amplitudes and phase differences of the magnetic fields in the frequency range of 0.1 to 20 Hz. Observation of the beads was performed on an inverted microscope, Eclipse Ti-S (Nikon), equipped with a PlanFluor 10x/0.30 objective. Images were time lapse recorded with a CCD camera (Hamamatsu) and subject to image analysis in NIH-ImageJ - a Java-based, open source software package.

TRAPPING BEADS ON THE WIRE, FORMING HELICES AND RINGS.

A simple method to generate circularly closed or helical field lines is a current carrying wire. According to the Biot-Savart law, the wire forms closed circular field lines around itself and should act as an elegant "field mould" for colloidal particle rings around its circumference. In general, a wire carrying a current I gives rise to a magnetic field at the position \mathbf{x} given by $\mathbf{H}_I(\mathbf{x}) = \frac{I}{4\pi} \int \frac{d\mathbf{x}_w}{ds} \times \frac{(\mathbf{x} - \mathbf{x}_w)}{\|\mathbf{x} - \mathbf{x}_w\|^3} ds$, where $\mathbf{x}_w(s)$ is the centerline position of the wire, s its arc-length and $\mathbf{t} = d\mathbf{x}_w/ds$ the wire's centerline tangent vector. In the simplest case of a straight long wire the expression simplifies to $\mathbf{H}_I(\mathbf{x}) = (I/2\pi r)\mathbf{e}_\phi$ with $r = |\mathbf{x}|$ the radial distance to the wire center, ϕ the azimuthal angle and $\mathbf{e}_\phi = \mathbf{e}_y \sin \phi - \mathbf{e}_x \cos \phi$ the azimuthal unit vector. In general, a spherical, paramagnetic bead placed in an external magnetic field $\mathbf{H}(\mathbf{x})$ has the free energy given by

$$W(\mathbf{x}) = -\frac{\mu_0}{2} \mathbf{m}(\mathbf{x}) \mathbf{H}(\mathbf{x}) = -\frac{\mu_0}{2} \chi_b V_b \mathbf{H}^2(\mathbf{x}), \quad (1)$$

where $\mathbf{m}(\mathbf{x}) \equiv \chi_b V_b \mathbf{H}(\mathbf{x})$ the magnetic moment of the bead, χ_b is the bead's susceptibility and V_b its volume. The bead experiences a magnetic gradient force

$$\mathbf{F} = -\partial W / \partial \mathbf{x} = \frac{\mu_0 \chi_b V_b}{2} \nabla (\mathbf{H}^2(\mathbf{x})). \quad (2)$$

We have built a simple setup consisting of a $50 \mu m$ (radius $25 \mu m$) thick long slender copper wire suspended above a glass surface, see Fig.1. After switching-on the current through the wire, superparamagnetic beads that previously sedimented onto the bottom surface by gravity interact with the field, Eq.2, and begin now to move towards the wire. They are attracted to the wire with a

force acting radially to the wire (in \mathbf{e}_r direction) given by

$$\mathbf{F} = -\frac{\mu_0 \chi_b V_b}{4\pi^2} \frac{I^2}{r^3} \mathbf{e}_r$$

If the wire is sufficiently close to the substrate plane (typically $< 100 - 150 \mu m$) and the current is high enough ($I > 100 mA$) the beads that have reached a close proximity to the wire begin to lift off the glass surface and attach to the bottom of the wire. This behavior sets in once the magnetic force overcomes the beads gravity force $F_g = (\rho_b - \rho_{sol}) g V_b \approx 0.22 pN$ with $(\rho_b - \rho_{sol}) \approx 0.5 g/ml$ the bead-solvent density contrast and $g = 9.8 \frac{m}{s^2}$ the gravity acceleration. Once they lift to the wire, the beads can be held on the wire with much smaller currents of the order $I = 2\pi (F_g r_w^3 / \mu_0 \chi_b V_b)^{1/2} \approx 35 mA$.

On the wire surface the beads form two dimensional clusters and short chains that progressively grow over time as a result of their dipole-dipole interactions. The dipole-dipole interactions tend to align the longer axes of chain-like clusters along the field lines, which in the case of simplest wire current field are pointing around the azimuthal direction of the cylindrical surface.

The shape and alignment of field lines and in turn the alignment of the clusters can be manipulated by invoking an additional external field \mathbf{H}_0 that superimposes with the wire field to give a total external field $\mathbf{H}(\mathbf{x}) = \mathbf{H}_0 + \mathbf{H}_I(\mathbf{x})$. In the first and simplest case, the uniform field points *parallel* to the wire axis $\mathbf{H}_0 = H_{0z} \mathbf{e}_z$. The total field in this case is given by

$$\mathbf{H}(r) = H_I(r) \mathbf{e}_\phi + H_{0z} \mathbf{e}_z \quad (3)$$

with $H_I(r) = I/2\pi r$. Superimposed, these two fields form helical field lines, with a pitch angle $\theta = \arctan(H_{0z}/H_I)$ that is followed by colloidal chains, see Fig.2.

By changing the proportion of the current I and the external field intensity H_{0z} one can manipulate the pitch angle θ of the helices, see Fig. 2. Due to the orthogonality of the two component fields, *i.e.* $\mathbf{e}_\phi \cdot \mathbf{e}_z = 0$, the energy (up to a constant term) and the gradient force resulting from Eq.(3) and Eq.(2) remain unchanged w.r.t. the pure wire field case ($H_{0z} = 0$). That is, while chains become reoriented by the presence of the *z-field*, single particles experience no change of trapping force or distribution on the surface.

In a second, more interesting case we impose an external field *orthogonal* to the wire axis (e.g. in the x direction)

$$\mathbf{H}(r, \phi) = H_I(r) \mathbf{e}_\phi + H_{0x} \mathbf{e}_x. \quad (4)$$

Note, that now the field combination loses azimuthal symmetry and depends both on the radial distance r and

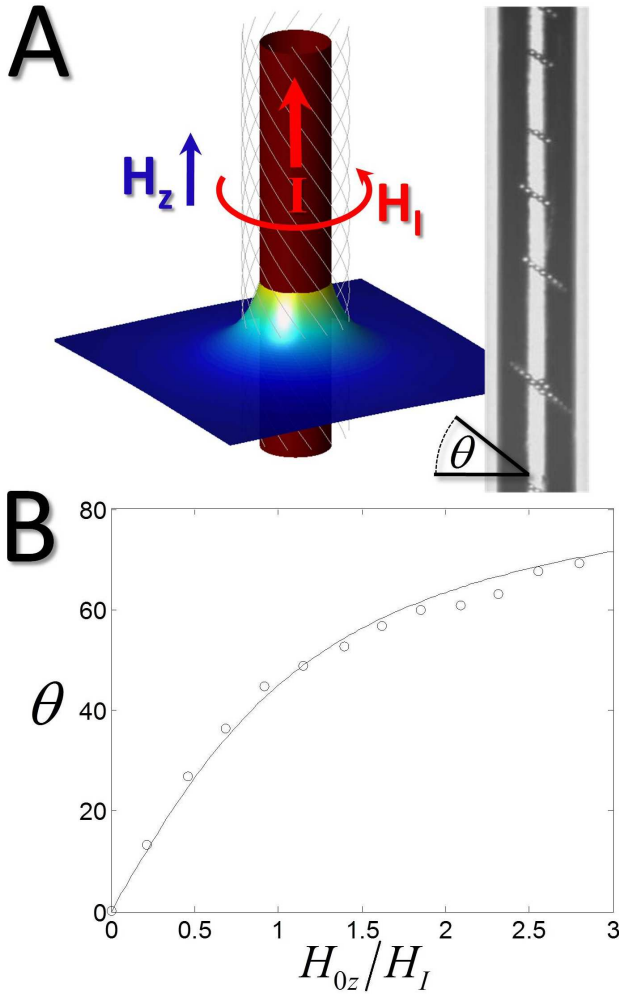


FIG. 2: A) A combination of the wire field and a z directed field induces helical field-lines (the total intensity H^2 is color coded) that guide the formation of circular arcs and helical filaments of varying pitch. B) The helix pitch as a function of external field over the wire field (circles) and the theoretical value (line).

the azimuthal angle ϕ , see Fig.3. A single bead in this field has the free energy

$$W(\phi, r) = -\frac{\chi_b \mu_0 V_b}{2} \left(\frac{I^2}{4\pi^2 r^2} - \frac{H_{0x} I}{\pi r} \cos \phi \right) + const. \quad (5)$$

From the azimuthal component $F_\phi = -(\partial W / \partial \phi) / r$ of the gradient force

$$F_\phi = \frac{\chi_b \mu_0 V_b}{2\pi} \frac{H_{0x} I}{r^2} \sin \phi \quad (6)$$

and its radial component $F_r = -(\partial W / \partial r)$

$$F_r = -\frac{\chi_b \mu_0 V_b}{4\pi^2} \frac{I^2}{r^3} \left(1 - \frac{2\pi H_{0x} r}{I} \cdot \cos \phi \right) \quad (7)$$

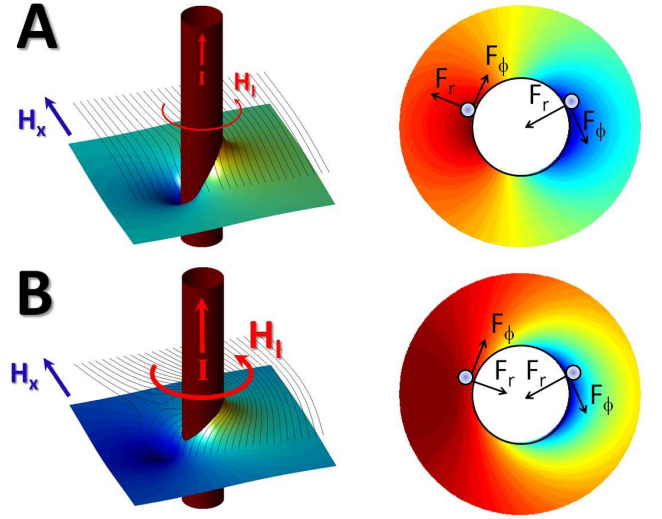


FIG. 3: The "magnetic merry-go-round trap" field configuration: A perpendicular field H_x superimposed to the wire field H_I generates a complex trapping field geometry. Left column: the total squared field strength H^2 , color code blue(red): low(high) H^2 . Right column: Potential energy of a superparamagnetic bead (color code blue : low energy) A) For a strong enough $H_x > H_I$ the normal component of the magnetic gradient force changes sign and is radially repulsive on one side. B) For sufficiently weak external field $H_x < H_I$ the trapping field is everywhere attractive towards the wire surface. The beads remain on the surface but experience azimuthal forces towards a single minimum energy position.

we see that depending on the magnitude of H_{0x} vs I and the angular position ϕ the wire surface can be either *attractive* or *repulsive* in the radial direction. In the following we will focus entirely on the weak external field, $H_{0x} < \frac{I}{2\pi r}$, where the wire is radially attractive[14], i.e. $F_r < 0$, and the beads are pressed onto the wire for any ϕ as in the case $H_{0x} = 0$. The presence of the symmetry breaking term $H_{0x} \mathbf{e}_x$ generates a preferred orientation for the bead on the wire surface, i.e. a free energy minimum at $\phi = \pi$. This induced energy minimum and the fact that beads as well as clusters follow it, will be used in the following to dynamically manipulate and transform clusters.

DYNAMICAL TRANSFORMATIONS BY HELICAL FIELDS AND SPINNING WAVES

The wire trap appears to be an elegant tool to form helices and rings on the wire, however the method meets practical some obstacles. Attracting beads to the wire from the bottom surface leads mostly to the formation of random, kinetically trapped, bulky clusters on the bottom side of the wire. Forming defect-free chain and ring structures via this process seems therefore very difficult and an unlikely process to happen spontaneously.

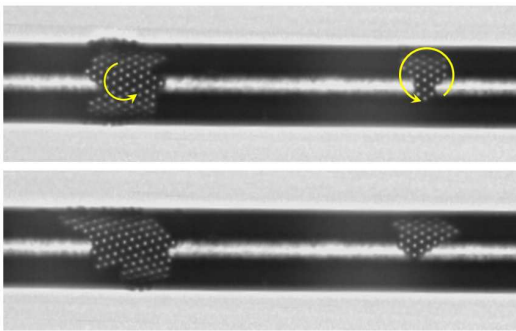


FIG. 4: Helically spinning fields lead to the formation of hexagonal clusters that spin with the field.

To remedy this problem our intuitive approach consists of applying additional *dynamic, time-dependent* fields to generate mixing of beads on the wire surface and transform them into linear chain configurations.

We have explored two different forms of dynamical external field perturbations: (a) Rotating helical field and (b) azimuthal spinning waves.

(a) *Rotary helical fields*, generated by an oscillating wire current $I \propto \sin \omega t$ and an out of phase longitudinal field $H_{0z} \propto \cos \omega t$.

In this case, at each spot of the wire the field is tangential and rotates around the cylindrical wire surface normal. We observe that cluster start to rotate, collide and form hexagonally ordered bigger clusters. At higher bead surface densities these rotating and growing clusters eventually cover the surface of the wire with a colloidal mono-layer. While this behavior is interesting in itself it does not lead to the desired elongation of clusters into chains.

(b) *Azimuthal spinning waves* ("Magnetic merry-go-round") - They are generated by a constant I and a *perpendicular oscillating external field* of the form:

$$\mathbf{H}_{0\perp}(t) = \mathbf{e}_x H_0 \sin \omega t + \mathbf{e}_y H_0 \cos \omega t. \quad (8)$$

In this case of rotating fields orthogonal to the wire the dynamical behavior is very much richer than in case (a). The fields of the wire and external field, as well as the induced dipolar fields between beads, dynamically interfere in an interesting manner. The perpendicular field $\mathbf{H}_{0\perp}(t)$ superimposes with the wire field $\mathbf{H}_I(\mathbf{x}) = \frac{I}{2\pi|\mathbf{x}|} \mathbf{e}_\phi$ and weakens it on one side but strengthens it on the other side of the wire leading to the formation of a wave-like field structure on the surface of the wire with a free energy of the form $W(\phi - \omega t, r)$ (Eq. 5) - , see Fig.3 and the previous section for the static case.

In the following we shall investigate how the propagation of spinning "merry-go-round" waves around the wire axis leads to a complex dynamical phenomenology, see Figs 5,6. The behavior of clusters in spinning fields

depends on two parameters : the field *spinning angular frequency* ω and the *relative field intensity* $h_0 = \frac{H_0}{H_I}$. We find that when the frequency of the spinning wave is sufficiently small $\omega < \omega_c$, with ω_c a critical frequency, one observes clusters of beads rotating uniformly with the field around the wire without a change of shape. In this "field locked" regime of slow field spinning, the clusters are following the field-maximum (i.e. the free energy minimum) on the wire surface with the same frequency but with a small constant angular lag. The clusters' angular lag behind the free energy minimum grows with increasing frequencies. From a critical frequency $\omega = \omega_c$ the clusters start to fall behind the potential more than a full turn. In this "unlocked" or "field skipping" regime, the clusters move with their own cluster frequency which is lower than the field frequency. During this motion the clusters occasionally skip the free energy maximum along their trajectory that leads them from one free energy minimum to the next one. For such supercritical frequencies $\omega \gtrsim \omega_c$ and at the same time large enough orthogonal field strengths, $h_0 \approx 1$, the clusters start to experience strong stretching forces at the free energy maxima. They in turn elongate and transform into slender, ring like structures. This transformation behavior becomes more frequent with growing frequency. However, with further increasing frequency the transformations gradually start to diminish for very rapid fields. Finally, for very high frequencies $\omega \gg \omega_c$ the spinning field becomes too fast and the clusters stop following the field dynamics. In the very fast field spinning regime the field does not affect the cluster shape significantly. Apart from small oscillations and a very slow azimuthal net rotation the clusters do not transform in this fast driving limit.

An example of the reshaping dynamics of transforming clusters at various frequencies is shown in Fig.5 and the diagram of transformation behavior in Fig.6. Interestingly switching from high frequencies back to lower ones, for sufficiently long time periods, can partially revert the effect of chain elongation, giving rise to crumpling and squeezing of clusters back into a more compact shape. This, in our case undesired, reverse buckling process can effectively be suppressed by abruptly stopping the spinning field (while maintaining the current in the wire constant), thus leaving the chain statically "frozen" in the desired elongated state.

ORIGIN OF CLUSTER TO CHAIN SHAPE TRANSFORMATION

The phenomenon of dynamic cluster elongation into chains is rather remarkable and deserves a theoretical investigation. We present it in the following Section for a simplified "dimer-toy model". Central to the model is the interplay of two dynamic phenomena that occur during the propagation of spinning waves around the wire. The

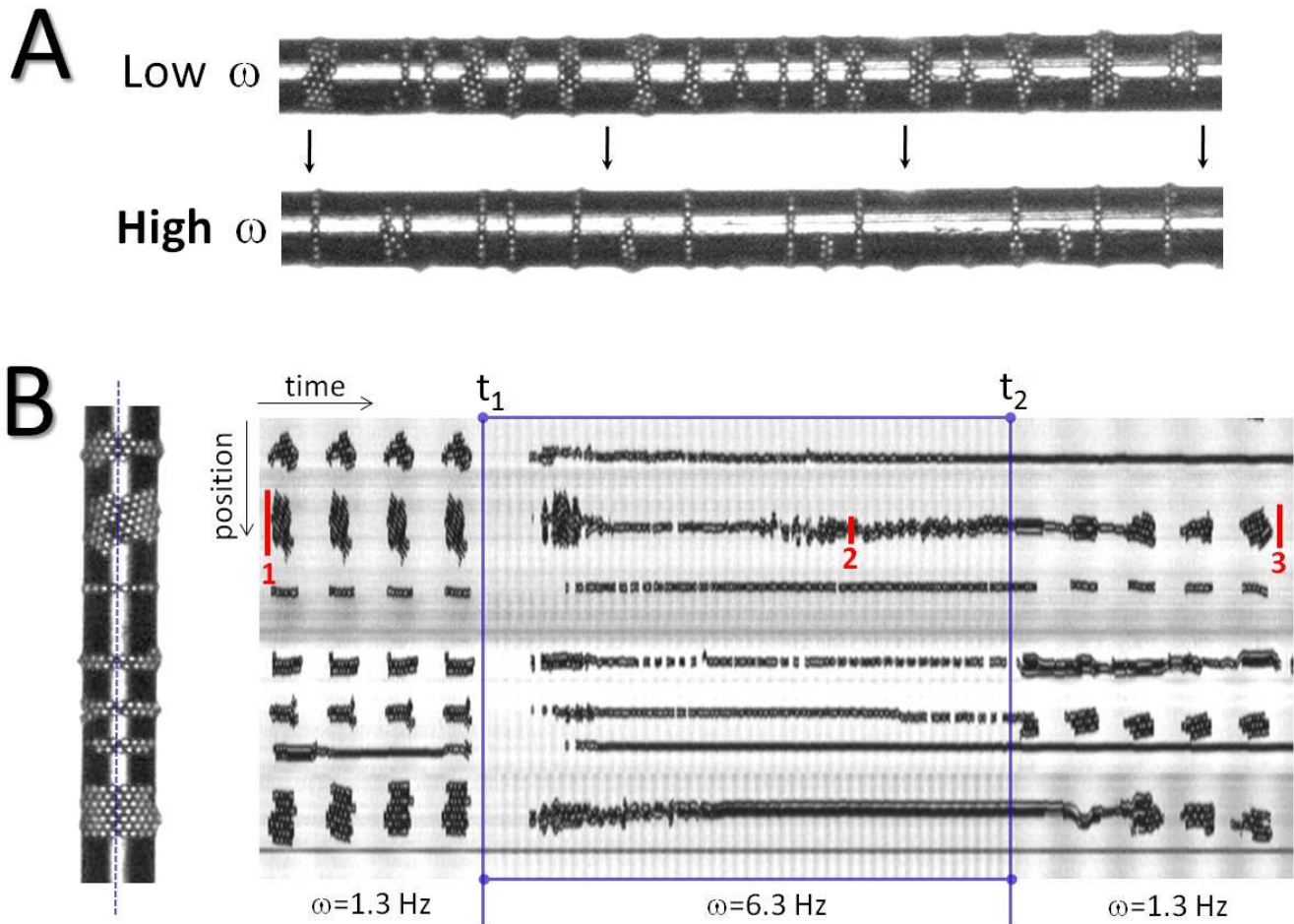


FIG. 5: Transformations under the merry-go-round, azimuthally spinning field: A) Amorphous clusters transform into elongated chains and rings upon the activation of the spinning field. B) A kymograph of the reshaping dynamics of several transforming clusters under the spinning field at various frequencies. The time interval of higher-frequency field spinning, between time t_1 and t_2 (blue box) the excitation leads to a lateral thinning and longitudinal elongation of the clusters. Reverting to a lower frequency spinning partially reverts the cluster elongation. The lateral width of a typical cluster at three different times is indicated by red lines.

first phenomenon for cluster transformation is the *locking / unlocking transition* of the cluster with respect to the rotating field. An elongating cluster should become unlocked and skip over the field barrier in order to become transformed. This transient event can lead to stretching and reshaping of the cluster. The second requirement for transformation is a *sufficiently high external field* at the point of barrier crossing. That is, under certain conditions, that will be clarified below, the crossing of the energy barrier involves a sufficiently destabilizing field able of tearing apart and rejoining the cluster into an elongated form.

During the cycle of potential skipping, the cluster experiences both, tension (at the potential maximum) and compression (at the potential minimum). This leads to the naive idea that elongation should be reverted, i.e. when the cluster elongates during the tension period it

should reshape back analogously into the more compact form during the compression phase. This reversibility is however prohibited by a third phenomenon that we call *configurational hysteresis*. As we show in the Appendix II, a magnetic chain with a side defect that is exposed to a cycling tension and compression will undergo a hysteresis in its shape. During the tension period the defect of the chain becomes unstable, smooths out and elongates but in the compression period it behaves asymmetrically. In particular, under appropriate dynamic conditions, the chain does not buckle back into the initial shape due to different barriers in both directions. Overall this asymmetric behavior tends to favor the elongation of magnetic clusters in general.

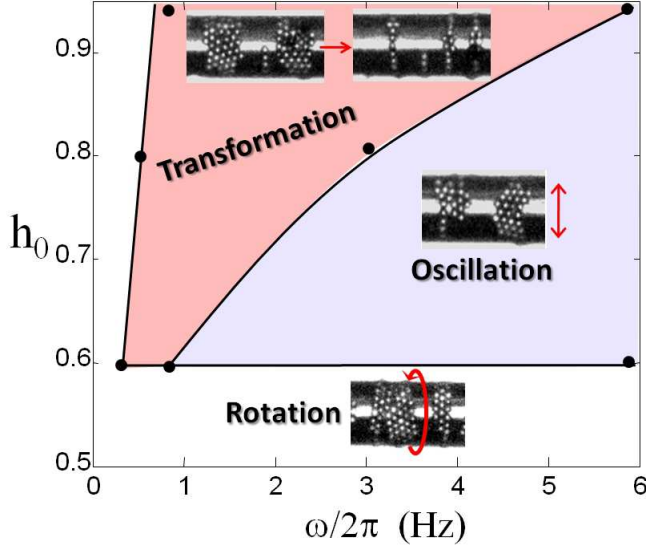


FIG. 6: Phase diagram of clusters in a spinning wave field as a function of the scaled external field $h_0 = \frac{H_0}{H_I}$ and the field spinning angular frequency ω .

Dimer Toy-Model for Cluster Transformation

Here the simplest analytically tractable model for cluster rearrangement - a simple two bead *dimer toy-model*. Of course, this simplest "proto" cluster cannot rearrange irreversibly beyond the two beads being simply pulled apart. However, the event of parts of the cluster coming apart is a central ingredient in all cluster transformations. Following the stretch-out and mutual separation of two sub-clusters, side chain beads pop-in and fill the gap between. In this sense studying the dimer toy-model has all of the ingredients for the precursor event of transformation - namely the dimer opening. With this interpretation of opening as a precursor, the dimer system mimics the phase-diagram of larger cluster transformation qualitatively rather well.

Consider two beads sitting on the wire (with the radius r_w) and acted upon the azimuthally spinning external field $\mathbf{H}_0(t) = \mathbf{H}_{0\perp}(\mathbf{x}, t) = \mathbf{e}_x H_0 \sin \omega t + \mathbf{e}_y H_0 \cos \omega t$, with bead coordinates $\mathbf{x}_{1,2} = (r_w, \varphi_{1,2})$ - see the geometry in Fig. 7. The two colloids interact with the external field and with each other via induced dipolar forces. The corresponding total free energy can be written as $W(\varphi_{1,2}, t) = W_0 + W_{dip} + W_{ev}$ with W_0 the interaction energy with the field given in Eq. (1), W_{dip} the the dipole-dipole interaction and $W_{ev}(\varphi_1 - \varphi_2)$ an excluded volume, short range, repulsive interaction between the beads. The total free energy W can be conveniently expressed as a function of the center of mass $\Phi = (\varphi_1 + \varphi_2)/2$ and the relative coordinate $\varphi = (\varphi_1 - \varphi_2)/2$.

In the limit of slow, viscosity-dominated motion (i.e. at zero Reynolds number) the dynamics is governed by

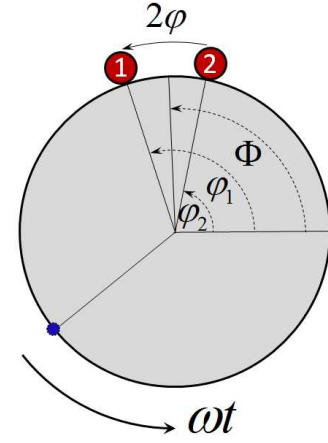


FIG. 7: The bead dimer model: The angular center of mass Φ of beads 1 and 2 follows the free energy minimum (blue dot) that is rotating with an angular velocity ω . The dimer's relative coordinate φ is an indicator for its opening and reshaping dynamics.

the Rayleigh dissipation function $R_{diss} = \frac{1}{2}\xi(\dot{\varphi}_1^2 + \dot{\varphi}_2^2)$. The friction coefficient $\xi \propto r_w^2 \eta$ is a phenomenological parameter that includes not only the solvent (dynamic) viscosity η , but also lubrication effects between the beads and the wire surface. For the calculations it is useful to introduce the center of mass angle coordinate in the field co-moving system $\Theta = \Phi + \omega t$. The dynamic equations of the two beads are given by $\partial R_{diss}/\partial \dot{\varphi} = -\partial W/\partial \varphi$ and $\partial R_{diss}/\partial \dot{\Theta} = -\partial W/\partial \Theta$ and explicitly written in Eqs. (14-15) of Appendix I. In the limiting case of $r_b/r_w \ll 1$ and $\varphi \gtrsim \varphi_{min} \approx r_b/r_w$ can be simplified to:

$$\dot{\Theta} = \omega + \omega_c \sin \Theta \quad (9)$$

$$\alpha \dot{\varphi} = -\frac{3}{2}[h_0^2 + 4] + 2h_0 \cos \Theta - \frac{9}{2}h_0^2 \cos 2\Theta. \quad (10)$$

Here $\omega_c = 2h_0/\alpha$ is a characteristic frequency, and $\alpha = 2\xi/\mu_0\chi_b H_I^2 V_b$ a characteristic timescale. By defining the effective "tilted wash-board" potential $U(\Theta) = -\omega\Theta + \omega_c \cos \Theta$ the co-moving center of mass Eq. (9) can also be written as $\dot{\Theta} = -\partial U/\partial \Theta$ [15].

Dimer Phase Diagram

We obtained the numerical solution of the full set of equations Eqs. (14-15) with an additional excluded volume, hard core interaction at short range, $\varphi \leq \varphi_{min}$. This allows us to study the opening dynamics (see Figs. 8) and obtain the full phase diagram (Fig.10) of the dimer-toy model. The numerical dimer-cluster solution, Fig 8,9 shows two regions of distinct dimer behavior that

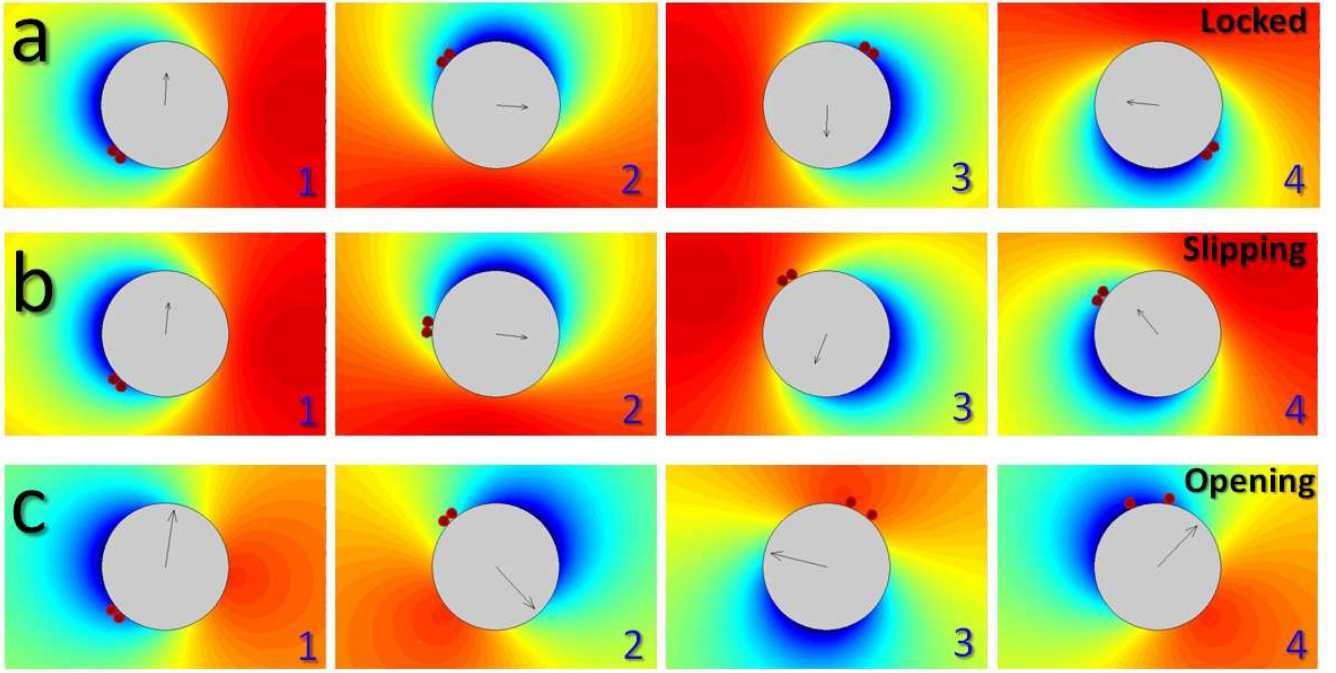


FIG. 8: Snapshots from the simulation of a dimer under spinning waves of various intensities and frequencies. The squared intensity of the total field (wire field + external field) is represented by the color code: high-field (low free energy) in blue, low-field (high free energy) in red. The beads tend to follow the free energy minimum (blue) for lower frequencies while lagging behind it at higher frequencies. Grey arrow: the direction of the external field. a) $h_0 = 0.5$, $\omega = 1$: the dimer is locked and moves with the field. b) $h_0 = 0.5$, $\omega = 2$: the field spins fast, the dimer lags behind the field but stays closed. c) $h_0 = 0.9$, $\omega = 3$: the dimer lags behind the field and opens up while skipping the free energy maximum.

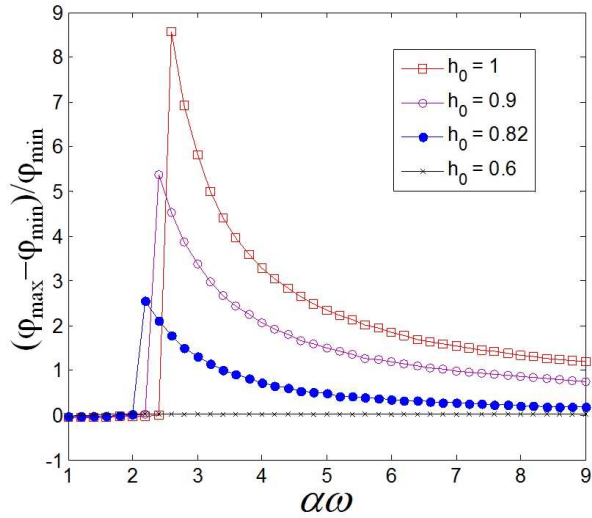


FIG. 9: The relative opening of the bead dimer for various h_0 as a function of the dimensionless driving frequency.

very much resemble the experimental cluster phase diagram, Fig.6. Within the region delimited by three characteristic lines in Fig. 10(1-3) the dimer opens sufficiently, i.e. order unity in terms of the bead's diameter, while outside that region the dimer does not open significantly.

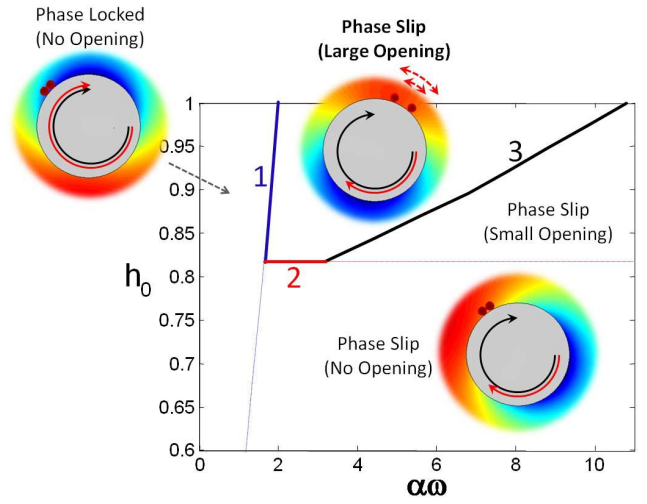


FIG. 10: Phase diagram of a bead dimer on the wire obtained by numeric integration of the equations of motion with an excluded volume term ensuring bead non-interpenetration. Black/red circular lines stand for the angular velocity of the field and the cluster respectively.

The position and shape of the boundary lines can be understood analytically from a closer analysis of Eqs.(9)

and (10) .

The *line 1* (blue line , Fig.10) delimits the region on the left where the dimer is field-locked and the region on the right where the cluster lags behind the field. Its approximate shape is obtained by studying the behavior of solutions to co-moving center of mass coordinate, Eq. (9). These solutions are $\Theta(t) = \text{cons.}$ for $\omega < \omega_c = 2h_0/\alpha$ (i.e. the cluster is locked to the field) and are unbounded for $\omega > \omega_c$ i.e. the cluster starts to move relative to the field coordinate system. Therefore the boundary line 1 is simply given by $h_0(\omega) = \alpha\omega/2$.

The second line, *line 2* (red line , Fig.10), can be understood by studying the relative coordinate Eq. (10). Along this delimiting line, the sign of the force acting on the relative coordinate flips from negative force (tending to close the dimer) to positive force (with a tendency to open it). The critical condition for line 2 is then given by setting $\dot{\varphi} = 0$ in Eq.(10) leading to the condition on the center of mass coordinate

$$\cos \Theta_{1,2} = \frac{4}{3h_0} \frac{1 \pm \sqrt{\frac{3}{4}h_0^2 - \frac{1}{2}}}{2}. \quad (11)$$

The requirement of a real solution implies $h_0 \geq h_{0,c} = (2/3)^{1/2} \approx 0.82$. Thus for h_0 beyond $h_{0,c}$ the dimer can open at some time point its cycle and $h_0 = (2/3)^{1/2}$ defines the delimiting line 2.

The *line 3* (black line , Fig.10) is given by the condition that the relative coordinate opens up sufficiently at some time point during the cycle for some t . The amount of opening in the phenomenological model , is to some extent arbitrary. In the phase diagram shown we chose a critical opening condition for an opening of order unity , i.e. $\varphi(t) > (3/2)\varphi_{\min}$. In this corner of the phase diagram, the dimer relative coordinate makes excursions from the closed state $\varphi(t) = \varphi_{\min}$ to some maximal value $\varphi(t) = \varphi_{\max}$. The size of this maximal excursion value φ_{\max} we can estimate from the typical time interval $\Delta t_{\text{open}} = t_2 - t_1$ for which a positive, dimer opening force f acts on the relative coordinate. The opening time interval is related to the maximal opening angle $\Delta\varphi = (1/\alpha) \int_{t_1}^{t_2} f(\Theta(t))dt \approx (1/2\alpha)\Delta t_{\text{ope}}$. Setting the opening angle to twice the minimal angle $\Delta\varphi = 2\varphi_{\min}$ (so that one additional bead would fit in between the maximally separated dimers), in the limit $\omega \gg \omega_c$ one estimates $\Delta t_{\text{open}} \approx (2\sqrt{2}h_0 - 1.6)/\omega$. The boundary line resulting from that is $h_0(\omega) \approx (1.6 + \alpha\omega\Delta\varphi)/2\sqrt{2}$ - in a satisfactory agreement with the line 3 (black) in Fig.10.

The region of the dimer toy-model phase diagram that is confined between these three critical lines (1-3) is also the region of interest for real large cluster transformation. To the left, bottom or right of this region, the cluster either does not open at all or does not open sufficiently for a transformation to occur. Quantitatively, the dimer-toy model overestimates the position of the line 2. In reality

the clusters transform at a lower external field $h_0^{\text{exp}} \sim 0.6$ as compared to the dimer simulation result $h_0^{\text{dim}} \sim 0.82$. Nevertheless, the shape of the transformation region is qualitatively captured and is rather similar to the experimental cluster transformation diagram, Fig.6, taken the simplicity and various approximations of the dimer-toy model.

In summary, we have seen that the dimer-toy model can phenomenologically explain the observed experimental observations. For a low field rotating frequency $\omega < \omega_c$ the center of mass of a cluster rotates uniformly and the beads are bound to stable clusters. For $\omega > \omega_c$ and a suitably large external field $h_0 > h_{0,c}$ the clusters are lagging behind the field and begin to tear apart. This tearing apart in the toy-model translates into a cluster-to-ring transformation as any two neighboring beads (or sub-clusters) in a bigger cluster would become stretched apart by the same mechanism. This in turn gives rise to gaps and holes between the sub-clusters, thus allowing lateral beads to pop-into the hole. If the time of stretching is sufficiently large a bead from the lateral side have enough time to enter between two stretched beads (or sub-clusters) with the tendency of forming elongated structures like rings.

CONCLUSION AND OUTLOOK

We have described a simple, yet robust method to trap and manipulate magnetic beads on a wire. While from equilibrium considerations we might expect rings and helical chains to form under such geometries in practice in a static field they are kinetically, notoriously improbable to form. However, by dynamically modulating the field of the wire with additional uniform, oscillatory external fields we have generated field geometries and dissipative forces that lead to a transformation of clusters into the desired linear structures. The method consists of "shaking down" colloidal structures in their free energy landscape via the trick of configurational hysteresis.

The generation of spinning magnetic waves has some similarities with propagating magnetic fields in flat geometries along planar magnetic garnets in rotating fields [20]. It allows to simply and inexpensively generate fluxes of magnetic particles along surfaces, a phenomenon that could have some interesting ramifications in particular for particle transport. Exploiting geometry of curved conductors of more complex shapes in combination with dynamic external field modulation opens an interesting playground for colloid world. Using for instance a helical wire combined with a perpendicularly rotating field would provide the spinning waves with an longitudinal component and enable pumping of particles along the wire surface [21].

The discussed system represents also a minimalistic way to self-assemble and operate a *magnetic micromo-*

tor: the wire being the stator and the colloidal cluster (or a single bead) acting as a rotor. A further down scaling of the system appears possible as thinner wires can more efficiently dissipate heat and carry larger currents allowing for similar trapping down to micron scales.

Finally, cross-linking the templated structures into self standing objects appears a very promising route in colloidal assembly. Helically cross-linked chains should become interesting magneto-responsive actuators when acted upon by larger fields.

Acknowledgements. We thank Christian Kreuter for kindly providing us with beads and the members of the M3 team for fruitful discussions. MLK thanks the members of the project ON171005 of the Institute of Physics, Belgrade for useful discussions.

APPENDIX

Appendix I: The free-energy and dynamical equations for two beads

The free-energy of two beads in an external field $\mathbf{H}(\mathbf{x})$ is $W = W_0 + W_{dip}$ where W_0 - given by Eq.(1), is the energy of the non-interacting beads. The dipole-dipole energy W_{dip} in leading order with respect to $\mathbf{H}(\mathbf{x})$ is given by

$$W_{dip} \approx -\mu_0 \chi_b V_b \mathbf{H}(\mathbf{x}_1) \hat{D}(\mathbf{x}_1, \mathbf{x}_2) \mathbf{H}(\mathbf{x}_2). \quad (12)$$

Here, $\mathbf{H}(\mathbf{x}) = \mathbf{H}_I(\mathbf{x}) + \mathbf{H}_0(t)$, $\hat{D}(\mathbf{x}_1, \mathbf{x}_2) = \Psi_{12}(1 - 3\hat{N}_{12})$, $\Psi_{12} = \chi_b V_b / 4\pi |\mathbf{x}_1 - \mathbf{x}_2|^3$ and $\hat{N}_{12} = \mathbf{n}_{12} \otimes \mathbf{n}_{12}$, $\mathbf{n}_{12} = (\mathbf{x}_1 - \mathbf{x}_2) / |\mathbf{x}_1 - \mathbf{x}_2|$. Two beads on the wire are characterized by angles φ_1, φ_2 . For further analysis it is convenient to use the relative coordinate $\varphi = (\varphi_1 - \varphi_2)/2$ and the center of mass coordinate $\Phi = (\varphi_1 + \varphi_2)/2$. The explicit expression for the free-energy reads ($\tilde{W} = W/(1/2)\mu_0 V_b H_I^2$)

$$\begin{aligned} \tilde{W}(\varphi, \Phi) = & const + 2h_0[1 + 2D(\varphi)] \cos \varphi \cos(\Phi + \omega t) \\ & - \frac{3}{2}h_0^2 D(\varphi) \cos 2(\Phi + \omega t) \\ & - \frac{3}{2}D(\varphi)[h_0^2 + (3 + \cos 2\varphi)], \end{aligned} \quad (13)$$

where $D(\varphi) = D_0(\sin \varphi_{\min}/\sin \varphi)^3$, $D_0 = \chi_b V_b / 4\pi d_b^3$ and the minimum contact angle of two beads is given by $\sin \varphi_{\min} = d_b/d_w$. By introducing the angle $\Theta = \Phi + \omega t$, that measures the mean coordinate in the field co-moving

frame, the equations for φ and Θ read

$$\begin{aligned} \alpha \dot{\varphi} = & -D(\varphi) \left\{ \sin 2\varphi + \frac{3 \cos \varphi}{2 \sin \varphi} [h_0^2 + 3 + \cos 2\varphi] \right\} \\ & + 2h_0 \left\{ [1 + 2D(\varphi)] \sin \varphi + 6D(\varphi) \frac{\cos^2 \varphi}{\sin \varphi} \right\} \cos \Theta \\ & - \frac{9}{2}D(\varphi) \frac{\cos \varphi}{\sin \varphi} \cos 2\Theta. \end{aligned} \quad (14)$$

$$\begin{aligned} \gamma(\dot{\Theta} - \omega) = & 2h_0 [1 + 2D(\varphi)] \cos \varphi \sin \Theta \\ & - 3h_0^2 D(\varphi) \sin 2\Theta, \end{aligned} \quad (15)$$

where $\alpha = 2\xi/\mu_0 \chi_b H_I^2 V_b$. Note, that the terms due to dipole-dipole interaction are proportional to $D(\varphi)$. In order to study the dynamics of the bead one should take into account its impenetrability, what formally implements a condition on φ that $\varphi > \varphi_{\min}$, i.e. the relative angle φ must be always larger than the contact angle of two beads $\sin \varphi_{\min} = r_b/r_w$. (In our experiments one has $\varphi_{\min} \approx r_b/r_w \approx 0.1$.) In the numerical calculations this effect is described by introducing a strong repulsive potential.

Since the dipole-dipole energy is proportional to $D(\varphi) < D_0$, where for our dynabeads one has $D_0 \approx 0.08$, then for $h_0 \gg D_0$ one can neglect the corresponding terms in Eq. (15). Since in our experiment $\varphi \gtrsim \varphi_{\min} \approx 0.1 - \varphi_{\min}$ is a minimal opening angle for the stretching (and entering of the third bead between the two beads), then in the first approximation one can retain in Eq. (15) the term with $\cos \varphi (\approx 1)$. The center of mass equation Eq. (15) is now reduced to the Eq.(9) in the main text. The equation for $\varphi(t)$ is also analogously simplified for $h_0 \gg D_0$ to Eq. (10).

The structure of solutions of Eq. (9) (which holds for $\varphi_{\min} \approx D_0 \approx 0.1$) depends on the dimensionless parameter $\kappa = \omega/\omega_c$ (with $\omega_c = 2h_0/\alpha$). For $\kappa < 1$ the solution is relaxation-like

$$\begin{aligned} \ln \frac{1 - \sqrt{1 - \kappa^2} + \kappa \tan \frac{\Theta}{2}}{1 + \sqrt{1 - \kappa^2} + \kappa \tan \frac{\Theta}{2}} \\ = \tau \sqrt{1 - \kappa^2} + const, \end{aligned} \quad (16)$$

where $\tau = \omega_c t$. Whatever initial conditions are, for large τ this solution goes to one of the minima $\Theta_{\min}^n = (2n + 1)\pi + \arcsin \kappa$ of $U(\Theta)$. This solution is characterized by the time averaged value $\langle \dot{\Theta} \rangle_t = 0$. For $\kappa > 1$ the solution is given by

$$\begin{aligned} \arctan \left[\frac{1}{\sqrt{\kappa^2 - 1}} \left(1 + \kappa \sqrt{\frac{1 - \cos \Theta}{1 + \cos \Theta}} \right) \right] \\ = \frac{\sqrt{\kappa^2 - 1}}{2} \omega_c t + const., \end{aligned} \quad (17)$$

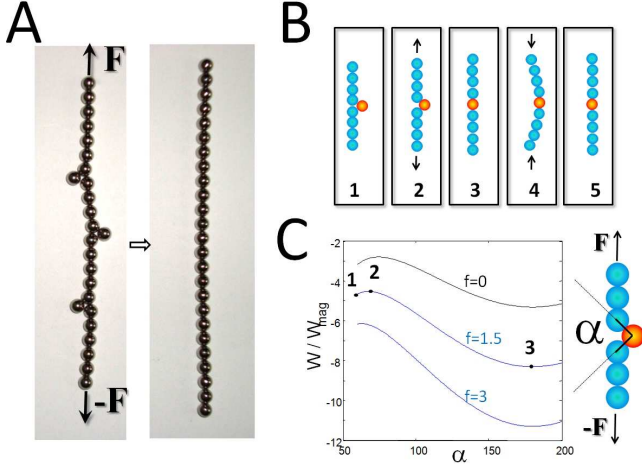


FIG. 11: A) A macroscopic (Neodymium) magnet chain straightens under a pulling force once a critical tension is reached. B) The recombination process of a side-chain defect becoming absorbed into the main chain during pulling (2,3). In the reverse cycle of pushing the ends with the same force, the chain does not revert but rather buckles on the large scale (3-5). C) The magnetic plus potential energy of a long, stretched, magnetic chain under various applied forces as function of the defect opening angle α . At a critical force the boundary minimum at $\alpha = 0$ becomes unstable and the chain relaxes in the straight chain, $\alpha = 180^\circ$ global energy minimum. Due to the asymmetry of the energy landscape the process is irreversible and exhibits a configurational hysteresis.

and it is characterized by $\langle \dot{\Theta} \rangle_t = \sqrt{\omega^2 - \omega_c^2}$, i.e. the "voltage-current" dependence is non-linear [19].

In the main text it is shown that *the opening regime is possible* if the condition $h_{0c} < h_0 < 1$ is fulfilled. As it was discussed above, the condition $h_0 < 1$ means that the beads are attracted to the wire if $H_0 < H_I$, while for $H_0 > H_I$ some beads in the rings (or clusters) are repelled from the wire and the self-assembly of rings is stopped. The condition for h_{0c} is obtained from Eq. (14) which describes the dynamics of the relative angle $\varphi > (\varphi_{\min})$ of two beads.

Appendix II: "Push-pull" hysteresis: macroscopic magnet chain example

As discussed in the main text, the lengthening of the aggregates can be associated with the popping-in transition of defects under tension.

Here we consider a simple model system: a chain of magnetic beads with a permanent magnetic moment m and a single side defect bead with radius R (see Fig 11). The chain is acted upon an external force F between its ends that mimics the tension when two beads in our "dimer-toy model", are sitting near the potential maxi-

mum or compression when they are at the minima.

We assume a linear chain consisting of $2N + 1$ beads along the y axis at positions $2R \left(0, \sin \frac{\alpha}{2} + k\right)$ and $2R \left(0, -\sin \frac{\alpha}{2} - l\right)$, $l, k = 0, \dots, N$ respectively and one single side chain bead at the middle position $2R \left(\cos \frac{\alpha}{2}, 0\right)$, and further that all the moments m are all pointing along the chain main axis (in the y direction $\mathbf{e}_y = (0, 1)$). Here α stands for the angle at the defect. The latter is $\alpha = 60^\circ$ if the 3 beads at the defect are in contact, i.e. the defect in a "closed state" and $\alpha > 60^\circ$ when the defect starts to open up and straighten. At $\alpha = 180^\circ$ the defect fully immerses into the main chain and has essentially disappeared. Therefore the angle α acts as a reaction coordinate representing the state of the defect.

The potential plus dipole-dipole interaction energy of the system is up to a α -independent constant

$$W = 2RF \sin \frac{\alpha}{2} - \frac{\mu_0 m^2}{2\pi} 2 \sum_{k=0}^{N-1} \frac{3(\mathbf{e}_y \cdot \mathbf{n}_k)^2 - 1}{r_k^3} - \frac{\mu_0 m^2}{2\pi} \sum_{l=0}^{N-1} \sum_{k=0}^{N-1} \frac{2}{r_{kl}^3} + const.$$

with the unit bond vectors $\mathbf{n}_k = \frac{1}{\sqrt{k^2 + 2k \sin \frac{\alpha}{2} + 1}} \left(-\cos \frac{\alpha}{2}, \sin \frac{\alpha}{2} + k\right)$ between the main chain and the defect particle, r_k the distance between the defect bead and the k -th main chain bead and r_{kl} the distance between the k -th and l -th bead in the top/bottom part of the main chain. This can be rewritten in terms of α :

$$\frac{W}{W_{mag}} = \frac{2RF}{W_{mag}} \sin \frac{\alpha}{2} + 2 \sum_{k=0}^{N-1} \frac{1 - 3 \left(\sin \frac{\alpha}{2} + k\right)^2 / d(\alpha, k)}{d(\alpha, k)^{3/2}} - \sum_{l=0}^{N-1} \sum_{k=0}^{N-1} \frac{2}{\left(2 \sin \frac{\alpha}{2} + k + l\right)^3}$$

with $W_{mag} = \frac{\mu_0 m^2}{4\pi R^3}$ and $d(\alpha, k) = k^2 + 2k \sin \frac{\alpha}{2} + 1$.

Note that even a chain with no tension applied can become unstable once a critical distance between the center-beads is surpassed. For a very long chain, $N \rightarrow \infty$, the summation can be performed numerically and the barrier is located at $\alpha = \alpha_c \approx 75^\circ$ (for a 2 bead main chain at $\alpha_c \approx 70^\circ$). This corresponds to a surface-to-surface opening distance of

$$\frac{D_c}{2R} = 2 \sin \left(\frac{\alpha_c}{2}\right) - 1 \approx 0.22$$

That is, for a main chain opening by a 22% of the bead diameter the defect becomes unstable.

For a simpler, analytically tractable case of only 3 bead recombination (2 in the main-chain and one recombining) with $N = 1$ and the energy simplifies to:

$$\frac{W}{W_{mag}} = fu - \frac{1}{4u^3} + 2(1 - 3u^2)$$

$$u = \sin \frac{\alpha}{2} \text{ and } f = \frac{2RF}{W_{mag}}$$

u is the half-distance between the main-chain beads. It goes from $u_1 = 1/2$ for $\alpha = 60^\circ$ and $u_2 = 1$ for $\alpha = 180^\circ$. It has extrema at

$$f + \frac{3}{4u^4} - 12u = 0$$

For vanishing force $f = 0$ we have the barrier at $u^* = 0.57435$. For nonzero f , in the two limiting cases $u = u_1$ and $u = u_2$ the barrier disappears for $f_1 = -6$ and $f_2 = 11.25$. The negative force f_1 corresponds to the critical tension for the side chain to "pop-in" and the positive f_2 corresponds to the buckling compression for the bead to "pop-out". The magnitude of the force necessary to create a defect is almost twice as large as the force needed to absorb the defect in the main chain.

* Electronic address: kulić@unistra.fr

- [1] L. E. Helseth, R.M. Muruganathan, Y. Zhang, and T. M. Fischer, Colloidal Rings in a Liquid Mixture, *Langmuir* 21,7271- (2005)
- [2] R. M. Erb, H. S. Son, B. Samanta, V. M. Rotello and B. B. Yellen, Magnetic assembly of colloidal superstructures with multipole symmetry, *Nature*, 457, 999 (2009)
- [3] D. Zerrouki, J. Baudry, D. Pine, P. Chaikin & J. Bibette, Chiral colloidal clusters, *Nature* 455, 380 (2008)
- [4] J. Yan, K. Chaudhary, S. C. Bae, J. A. Lewis, and S. Granick, Colloidal Ribbons and Rings from Janus Magnetic Rods, *Nature Comm.* 4, 1516 (2013)
- [5] J. E. Martin, R. A. Anderson, R. L. Williamson, *J. Chem. Phys.* **118**, 1557 (2003); J. E. Martin, E. Venturini, G. L. Gulley, J. Williamson, *Phys. Rev.* **E 69**, 021508-1 (2004)
- [6] I.M. Kulić and M.L. Kulić. Self-Assembly of Colloidal Superstructures in Coherently Fluctuating Fields. *Phys. Rev. Lett.*, 111, 198301 (2013); Theory of coherent van der Waals matter. *Phys. Rev. E* 90, 062313 (2014).
- [7] N. Osterman, I. Poberaj, J. Dobnikar, D. Frenkel, P. Ziherl, D. Babić, Field-induced self-assembly of suspended colloidal membranes, *Phys. Rev. Lett.* **103**, 228301 (2009)
- [8] G. Kokot, J.S. Zemljčić, U. Batista and D. Babić, Magnetically Self-Assembled Colloidal Three-Dimensional Structures as Cell Growth Scaffold. *Langmuir* 31, 9576 (2015).
- [9] Pietro Tierno, Recent advances in anisotropic magnetic colloids: realization, assembly and applications, *Phys. Chem. Chem. Phys.*, 16, 23515 (2014)
- [10] J. E. Martin and A. Snezhko, Driving self-assembly and emergent dynamics in colloidal suspensions by time-dependent magnetic fields, *Rep. Prog. Phys.* 76, 126601 (2013)
- [11] A. Snezhko, I. S. Aranson, and W.-K. Kwok, Surface Wave Assisted Self-Assembly of Multidomain Magnetic Structures, *Phys. Rev. Lett.* 96, 078701 (2006)
- [12] A. P. Philipse and D. Maas, Magnetic Colloids from Magnetotactic Bacteria: Chain Formation and Colloidal Stability, *Langmuir*, 18, 9977 (2002)
- [13] Dynabeads M-450, uncoated; DYNAL PARTICLES AS, <http://www.dynalbiotech.com>
- [14] However, notice that in the opposite limit, not considered here further, $H_{0x} > \frac{I}{2\pi r}$ there is an interesting phenomenon of formation of a *minimum squared field* line (with a spacial minimum of \mathbf{H}^2). This line is parallel to the wire (and fully outside of it) at a distance $r_{trap} = \frac{I}{2\pi H_{0x}} > r_w$. The latter could be used to effectively trap diamagnetic beads ($\chi_b < 0$) like non-magnetic cavities in a ferrofluid or suspended superconducting beads.
- [15] Note, that the equation for $\Theta(t)$ is similar to the Josephson equation for the dynamics of the superconducting phase difference in a resistive current-driven π -junction circuit [19]. The above quantities $\dot{\Theta}$, ω and $\omega_c \sin \Theta$ play the role of voltage (on the resistive element), driven external current and Josephson current, respectively. The equation appears also in other systems involving particle coupling to rotating fields and this principle has been used for micro-sensing by optical torque driven beads [16].
- [16] F. Pedaci, Z. Huang, M. van Oene, S. Barland and N. H. Dekker, Excitable particles in an optical torque wrench. *Nature Physics* 7, 259 (2011)
- [17] Christian Kreuter, PhD Thesis, Konstanz Univ., Diss. (2012)
- [18] K. Zahn, R. Lenke and G. Maret, Two-Stage Melting of Paramagnetic Colloidal Crystals in Two Dimensions, *Phys. Rev. Lett.* 82, 2721 (1999); H. König, R. Hund, K. Zahn and G. Maret, Experimental realization of a model glass former in 2D, *Eur. Phys. J. E* 18, 287–293 (2005)
- [19] L. N. Bulaevskii, V. V. Kuzii, A. I. Sobyenin, Superconducting system with weak coupling to the current in the ground state, *JETP Letters*, **25**, 290 (1977); On the possibility of the spontaneous magnetic flux in a Josephson junction containing magnetic impurities, *Solid State Commun.*, **25**, 1053 (1978)
- [20] P. Tierno, T. H. Johansen, and T. M. Fischer, Localized and Delocalized Motion of Colloidal Particles on a Magnetic Bubble Lattice. *Phys. Rev. Lett.* 99, 038303 (2007); P. Tierno, F. Sagués, T. H. Johansen and T.M. Fischer, Colloidal transport on magnetic garnet films. *Phys. Chem. Chem. Phys.* 11, 9615 (2009)
- [21] I.M. Kulić and M.L. Kulić, In preparation.